

Steering paradox for Einstein–Podolsky–Rosen argument and its extended inequality

TIANFENG FENG,^{1,†} CHANGLIANG REN,^{2,5,†} QIN FENG,^{1,†} MAOLIN LUO,¹ XIAOGANG QIANG,³
JING-LING CHEN,^{4,6}  AND XIAOQI ZHOU^{1,7}

¹State Key Laboratory of Optoelectronic Materials and Technologies and School of Physics, Sun Yat-sen University, Guangzhou 510275, China

²Key Laboratory of Low-Dimensional Quantum Structures and Quantum Control of Ministry of Education, Key Laboratory for Matter Microstructure and Function of Hunan Province, Department of Physics and Synergetic Innovation Center for Quantum Effects and Applications, Hunan Normal University, Changsha 410081, China

³National Innovation Institute of Defense Technology, AMS, Beijing 100071, China

⁴Theoretical Physics Division, Chern Institute of Mathematics, Nankai University, Tianjin 300071, China

⁵e-mail: renchangleiang@hunnu.edu.cn

⁶e-mail: chenjl@nankai.edu.cn

⁷e-mail: zhouxq8@mail.sysu.edu.cn

Received 6 October 2020; revised 16 March 2021; accepted 17 March 2021; posted 19 March 2021 (Doc. ID 411033); published 20 May 2021

The Einstein–Podolsky–Rosen (EPR) paradox is one of the milestones in quantum foundations, arising from the lack of a local realistic description of quantum mechanics. The EPR paradox has stimulated an important concept of “quantum nonlocality,” which manifests itself in three types: quantum entanglement, quantum steering, and Bell’s nonlocality. Although Bell’s nonlocality is more often used to show “quantum nonlocality,” the original EPR paradox is essentially a steering paradox. In this work, we formulate the original EPR steering paradox into a contradiction equality, thus making it amenable to experimental verification. We perform an experimental test of the steering paradox in a two-qubit scenario. Furthermore, by starting from the steering paradox, we generate a generalized linear steering inequality and transform this inequality into a mathematically equivalent form, which is friendlier for experimental implementation, i.e., one may measure the observables only in the x , y , or z axis of the Bloch sphere, rather than other arbitrary directions. We also perform experiments to demonstrate this scheme. Within the experimental errors, the experimental results coincide with theoretical predictions. Our results deepen the understanding of quantum foundations and provide an efficient way to detect the steerability of quantum states. © 2021 Chinese Laser Press

<https://doi.org/10.1364/PRJ.411033>

1. INTRODUCTION

The quantum paradox has provided an intuitive way to reveal the essential difference between quantum mechanics and classical theory. In 1935, by considering a continuous-variable entangled state $\Psi(x_1, x_2) = \int_{-\infty}^{+\infty} e^{ip(x_1 - x_2 + x_0)/\hbar} dp$, Einstein, Podolsky, and Rosen (EPR) proposed a thought experiment to highlight a famous paradox [1]: either the quantum wavefunction does not provide a complete description of physical reality, or measuring one particle from a quantum entangled pair instantaneously affects the second particle regardless of how far apart the two entangled particles are. The EPR paradox has revealed a sharp conflict between local realism and quantum mechanics, thus triggering the investigation of nonlocal properties of quantum entangled states. Soon after the publication of the EPR paper, Schrödinger made an immediate response by introducing the term “steering” to depict “the spooky action at a distance” that was mentioned in the EPR argument [2]. According to Schrödinger, “steering” reflects a nonlocal

phenomenon that, in a bipartite scenario, describes the ability of one party, say Alice, to prepare the other party’s, say Bob’s, particle in different quantum states by simply measuring her own particle using different settings. However, the notion of steering did not gain much attention or development until 2007, when Wiseman *et al.* gave a rigorous definition using concepts from quantum information [3].

Undoubtedly, the EPR paradox is a milestone in quantum foundations, as it has opened the door of “quantum nonlocality.” In 1964, Bell made a distinct response to the EPR paradox by showing that quantum entangled states may violate Bell’s inequality, which hold for any local-hidden-variable model [4]. This indicates that local-hidden-variable models cannot reproduce all quantum predictions, and the violation of Bell’s inequality by entangled states directly implies a kind of nonlocal property—Bell’s nonlocality. Since then, Bell’s nonlocality has achieved rapid and fruitful development in two directions [5]. (i) On one hand, more and more Bell’s inequalities have been

introduced to detect Bell’s nonlocality in different physical systems, e.g., the Clauser–Horne–Shimony–Holt (CHSH) inequality for two qubits [6], the Mermin–Ardehali–Belinskii–Klyshko (MABK) inequality for multipartite qubits [7], and the Collins–Gisin–Linden–Masser–Popescu inequality for two qudits [8]. (ii) On the other hand, some novel quantum paradoxes, or the all-versus-nothing (AVN) proofs, have been suggested to reveal Bell’s nonlocality without inequalities. Typical examples are the Greenberger–Horne–Zeilinger (GHZ) paradox [9] and the Hardy paradox [10]. Experimental verifications of Bell’s nonlocality have also been carried out; for instance, Aspect *et al.* successfully made the first observation of Bell’s nonlocality with the CHSH inequality [11], Pan *et al.* tested the three-qubit GHZ paradox in a photon-based experiment [12], and very recently, Luo *et al.* tested the generalized Hardy paradox for multi-qubit systems [13].

Despite being developed from the EPR paradox, Bell’s nonlocality does not directly correspond to the EPR paradox. As pointed out in Ref. [3], inspired by the EPR argument, one can derive three types of “quantum nonlocality”: quantum entanglement, quantum steering, and Bell’s nonlocality. The original EPR paradox is actually a special case of quantum steering [14]. Although quantum steering has been experimentally demonstrated in various quantum systems [15–24], all of these experiments just indirectly illustrate the EPR paradox, in which most of them are based on statistical inequalities. Here the direct illustration of a quantum paradox means that we can find a contradiction equality for this paradox and demonstrate it (Ref. [16] is an AVN proof but not a contradiction equality). For example, (i) the GHZ paradox [9] can be formulated as a contradiction equality “+1 = -1”, where “+1” represents the prediction of the local-hidden-variable model, while “-1” is the quantum prediction. Thus, if one observes the value of “-1” by some quantum technologies in experiments, then the GHZ paradox is demonstrated. (ii) The formulation of the Hardy paradox [10] is given as follows: under some certain Hardy-type constraints for probabilities $P_1 = P_2 = \dots = P_N = 0$, any local-hidden-variable model predicts a zero probability (i.e., $P_{\text{succ}} = 0$), while quantum prediction is $P_{\text{succ}} > 0$, where P_{succ} is the success probability of a specific event. Upon successfully measuring the desired non-zero success probability under the required Hardy constraints, one verifies the Hardy paradox. A natural question arises as to whether the EPR paradox, which excludes any local-hidden-state (LHS) model, can be illustrated in a direct way just like the GHZ or Hardy paradox.

The purpose of this paper is two-fold. (i) Based on our previous results of the steering paradox “2 = 1” [25], we present a generalized steering paradox “ $k = 1$.” We also perform an experiment to illustrate the original EPR paradox through demonstrating the steering paradox “2 = 1” in a two-qubit scenario. (ii) A steering paradox can correspond to an inequality (e.g., the two-qubit Hardy paradox may correspond to the well-known CHSH inequality) [26,27], and from the steering paradox “ $k = 1$,” we generate a generalized linear steering inequality (GLSI), which naturally includes the usual LSI as a special case [3,15]. Also, the GLSI can be transformed into a mathematically equivalent form, but is friendlier for experimental implementation, i.e., one may measure the observables

only in the x , y , or z axis of the Bloch sphere, rather than other arbitrary directions. We also experimentally test quantum violations of the GLSI, which shows that it is more powerful than the usual one in detecting the steerability of quantum states.

2. EPR PARADOX AS A STEERING PARADOX “ $k = 1$ ”

Following Ref. [25], let us consider an arbitrary two-qubit pure entangled state $\rho_{AB} = |\Psi(\alpha, \varphi)\rangle\langle\Psi(\alpha, \varphi)|$ shared by Alice and Bob. Using the Schmidt decomposition, i.e., in the \hat{z} -direction representation, the wave-function $|\Psi(\alpha, \varphi)\rangle$ may be written as

$$|\Psi(\alpha, \varphi)\rangle = \cos \alpha|00\rangle + e^{i\varphi} \sin \alpha|11\rangle, \quad (1)$$

with $\alpha \in (0, \pi/2)$ and $\varphi \in [0, 2\pi]$. For the same state Eq. (1), in the general \hat{n} -direction decomposition, one may recast it to

$$|\Psi(\alpha, \varphi)\rangle = |+\hat{n}\rangle|\chi_{+\hat{n}}\rangle + |-\hat{n}\rangle|\chi_{-\hat{n}}\rangle, \quad (2)$$

where $|\pm\hat{n}\rangle$ are the eigenstates of the operator $\hat{P}_a^{\hat{n}} = [\mathbb{1} + (-1)^a \vec{\sigma} \cdot \hat{n}]/2$ denoting Alice’s projective measurement on her qubit along the \hat{n} direction with measurement outcomes a ($a = 0, 1$), $\mathbb{1}$ is the identity matrix, $\vec{\sigma} = (\sigma_x, \sigma_y, \sigma_z)$ is the vector of Pauli matrices, and $|\chi_{\pm\hat{n}}\rangle = \langle\pm\hat{n}|\Psi(\alpha, \varphi)\rangle$ are the collapsed pure states (unnormalized) for Bob’s qubit.

By performing a projective measurement on her qubit along the \hat{n} direction, Alice, by wave-function collapse, steers Bob’s qubit to the pure states $\rho_a^{\hat{n}} = \tilde{\rho}_a^{\hat{n}}/\text{tr}(\tilde{\rho}_a^{\hat{n}})$ with the probability $\text{tr}(\tilde{\rho}_a^{\hat{n}})$; here $\tilde{\rho}_a^{\hat{n}} = \text{tr}_A[(\hat{P}_a^{\hat{n}} \otimes \mathbb{1})\rho_{AB}]$ are the so-called Bob’s unnormalized conditional states, and $\rho_a^{\hat{n}}$ are the normalized ones [3]. In a two-setting steering protocol $\{\hat{z}, \hat{x}\}$, if Bob’s four unnormalized conditional states can be simulated by an ensemble $\{\mathcal{G}_\xi \rho_\xi\}$ of the LHS model, then these may be described as [25]

$$\tilde{\rho}_0^{\hat{z}} = \cos^2 \alpha |0\rangle\langle 0| = \mathcal{G}_1 \rho_1, \quad (3a)$$

$$\tilde{\rho}_1^{\hat{z}} = \sin^2 \alpha |1\rangle\langle 1| = \mathcal{G}_2 \rho_2, \quad (3b)$$

$$\tilde{\rho}_0^{\hat{x}} = (1/2)|\chi_+\rangle\langle\chi_+| = \mathcal{G}_3 \rho_3, \quad (3c)$$

$$\tilde{\rho}_1^{\hat{x}} = (1/2)|\chi_-\rangle\langle\chi_-| = \mathcal{G}_4 \rho_4, \quad (3d)$$

where $|\chi_\pm\rangle = \cos \alpha|0\rangle \pm e^{i\varphi} \sin \alpha|1\rangle$ are normalized pure states, ρ_i are hidden states, and \mathcal{G}_i represent the corresponding probabilities in the ensemble. They satisfy the constraint $\sum_\xi \mathcal{G}_\xi \rho_\xi = \rho_B = \text{tr}_A(\rho_{AB})$, where ρ_B is the reduced density matrix of Bob. On the other hand, since $\tilde{\rho}_0^{\hat{z}} + \tilde{\rho}_1^{\hat{z}} = \rho_B$ and $\text{tr}(\rho_B) = 1$, if we sum up terms in Eq. (3) and take the trace, we arrive at the contradiction “2 - 1,” which represents the EPR paradox in the two-setting steering protocol.

Here we show that a more general steering paradox “ $k = 1$ ” can be similarly obtained if one considers a k -setting steering scenario $\{\hat{n}_1, \hat{n}_2, \dots, \hat{n}_k\}$, in which Alice performs k projective measurements on her qubit along \hat{n}_j directions (with $j = 1, 2, \dots, k$). For each projective measurement $\hat{P}_a^{\hat{n}_j}$, Bob obtains the corresponding unnormalized pure states $\tilde{\rho}_a^{\hat{n}_j}$. Suppose these states can be simulated by the LHS model; then one may obtain the following set of $2k$ equations:

$$\tilde{\rho}_0^{\hat{n}_j} = \sum_\xi \mathcal{G}_\xi \rho_\xi(0|\hat{n}_j, \xi) \rho_\xi, \quad (4a)$$

$$\hat{\rho}_1^{\hat{n}_j} = \sum_{\xi} \mathcal{G}(1|\hat{n}_j, \xi) \mathcal{G}_{\xi} \rho_{\xi}, j = 1, 2, \dots, k. \quad (4b)$$

Since $\hat{\rho}_a^{\hat{n}_j}$ are proportional to pure states, the sum of the right-hand side of Eq. (4) actually contains only one ρ_{ξ} , as we have seen for Eq. (3). Furthermore, due to the relations $\hat{\rho}_0^{\hat{n}_j} + \hat{\rho}_1^{\hat{n}_j} = \rho_B$ and $\sum_{\xi=1}^{2k} \mathcal{G}_{\xi} \rho_{\xi} = \rho_B$, and by taking the trace of Eq. (4), one immediately has the steering paradox “ $k = 1$.”

Experimentally, we test the EPR paradox for a two-qubit system in the simplest case of $k = 2$. To this aim, we need to perform measurements leading to four quantum probabilities. The first one is $P_1^{\text{QM}} = \text{tr}[\hat{\rho}_0^{\hat{z}}|0\rangle\langle 0|] = \cos^2\alpha$, which is obtained from Bob by performing the projective measurement $|0\rangle\langle 0|$ on his unnormalized conditional state as in Eq. (3a). Similarly, from Eqs. (3b)–(3d), one has $P_2^{\text{QM}} = \text{tr}[\hat{\rho}_1^{\hat{z}}|1\rangle\langle 1|] = \sin^2\alpha$, $P_3^{\text{QM}} = \text{tr}[\hat{\rho}_0^{\hat{x}}|\chi_+\rangle\langle \chi_+|] = 1/2$, and $P_4^{\text{QM}} = \text{tr}[\hat{\rho}_1^{\hat{x}}|\chi_-\rangle\langle \chi_-|] = 1/2$. Consequently, the total quantum prediction is $P_{\text{total}}^{\text{QM}} = \sum_{i=1}^4 P_i^{\text{QM}} = 2$, which contradicts the LHS model prediction “1.” If within the experimental measurement errors one obtains a value $P_{\text{total}}^{\text{QM}} \approx 2$, then the steering paradox “ $2 = 1$ ” is demonstrated.

3. GENERALIZED LINEAR STEERING INEQUALITY

Just as Bell’s inequalities may be derived from the GHZ and Hardy paradoxes [26,27], this is also the case for the EPR paradox. In turn, from the steering paradox “ $k = 1$,” one may derive a k -setting GLSI as follows: in the steering scenario $\{\hat{n}_1, \hat{n}_2, \dots, \hat{n}_k\}$, Alice performs k projective measurements along \hat{n}_j directions. Upon preparing the two-qubit system in the pure state $|\Psi(\theta, \phi)\rangle$ (note that this is not $|\Psi(\alpha, \varphi)\rangle$ and here $|\Psi(\theta, \varphi)\rangle$ is used to derive the inequality), for each measurement $\hat{P}_a^{\hat{n}_j}$, Bob has corresponding normalized pure states as $\rho_a^{\hat{n}_j}(\theta, \phi) = \hat{\rho}_a^{\hat{n}_j} / \text{tr}(\hat{\rho}_a^{\hat{n}_j})$, where $\hat{\rho}_a^{\hat{n}_j} = \text{tr}_A[(\hat{P}_a^{\hat{n}_j} \otimes \mathbb{1})|\Psi(\theta, \phi)\rangle\langle \Psi(\theta, \phi)|]$, with $a = 0, 1$. Then the k -setting GLSI is given by (see Appendix A)

$$S_k(\theta, \phi) = \sum_{j=1}^k \left[\sum_{a=0}^1 P(A_{n_j} = a) \langle \rho_a^{\hat{n}_j}(\theta, \phi) \rangle \right] \leq C_{\text{LHS}}, \quad (5)$$

which is a (θ, ϕ) -dependent inequality, where C_{LHS} is the classical bound determined by the maximal eigenvalue of $S_k(\theta, \phi)$ for the given values of θ and ϕ , $P(A_j = a)$ is the probability of the j th measurement of Alice with outcome a , and $\rho_a^{\hat{n}_j}(\theta, \phi) = |\chi_{\pm}^j(\theta, \phi)\rangle\langle \chi_{\pm}^j(\theta, \phi)|$ corresponds to Bob’s projective measurements. This inequality can be used to detect the steerability of two-qubit pure or mixed states.

The GLSI has two remarkable advantages over the usual LSI [15]. (i) Based on its own form as in the inequality (5), the GLSI includes naturally the usual LSI as a special case, and thus can detect more quantum states. In particular, the GLSI can detect the steerability for all pure entangled states Eq. (1) in the whole region $\alpha \in (0, \pi/2)$, at variance with the usual LSI, which fails to detect EPR steering for some regions of α close to zero [28]. (ii) The use of GLSI reduces the numbers of experimental measurements and improves the experimental

accuracy. This may be seen as follows: with the usual k -setting LSI, Bob needs to perform k measurements in different k directions, for different input states ρ_{AB} . This is experimentally challenging since it may be hard to suitably tune the setup for all k directions. However, with the GLSI, one may solve this issue using the Bloch realization $|\chi_{\pm}^j\rangle\langle \chi_{\pm}^j| = (\mathbb{1} + \vec{\sigma} \cdot \hat{m}_{\pm}^j)/2$, which transforms the GLSI to an equivalent form where Bob needs to perform measurements only along the \hat{x} , \hat{y} , and \hat{z} directions of the Bloch sphere, which are independent on the input states (see Appendix A).

To be more specific, we give an example of the three-setting GLSI from the inequality (5), where Alice’s three measuring directions are $\{\hat{x}, \hat{y}, \hat{z}\}$. Then we immediately have

$$S_3 = P(A_x = 0)\langle \chi_+ \rangle \langle \chi_+ | + P(A_x = 1)\langle \chi_- \rangle \langle \chi_- | \\ + P(A_y = 0)\langle \chi'_+ \rangle \langle \chi'_+ | + P(A_y = 1)\langle \chi'_- \rangle \langle \chi'_- | \\ + P(A_z = 0)\langle |0\rangle \langle 0| + P(A_z = 1)\langle |1\rangle \langle 1| \leq C_{\text{LHS}}, \quad (6)$$

with $|\chi_{\pm}\rangle = \cos\theta|0\rangle \pm e^{i\phi}\sin\theta|1\rangle$, $|\chi'_{\pm}\rangle = \cos\theta|0\rangle \mp e^{i\phi}\sin\theta|1\rangle$, $C_{\text{LHS}} = \text{Max}\left\{\frac{3+C_{\pm}}{2}, \frac{3+C_{\pm}}{2}\right\}$, and $C_{\pm} = \sqrt{4 \pm 4\cos 2\theta + \cos 4\theta}$. The equivalent three-setting steering inequality is given by (see Appendix B)

$$S'_3(\theta, \phi) = \sin 2\theta \cos \phi \langle A_x \sigma_x \rangle - \sin 2\theta \cos \phi \langle A_y \sigma_y \rangle \\ + \sin 2\theta \sin \phi \langle A_x \sigma_y \rangle + \sin 2\theta \sin \phi \langle A_y \sigma_x \rangle \\ + \langle A_z \sigma_z \rangle + 2 \cos 2\theta \langle \sigma_z \rangle \leq C'_{\text{LHS}}, \quad (7)$$

with $C'_{\text{LHS}} = \text{Max}\{C_+, C_-\}$. Obviously, by taking $\theta = \pi/4$ and $\phi = 0$, the inequality (7) reduces to the usual three-setting LSI in the form [15]

$$S'_3(\pi/4, 0) = \langle A_x \sigma_x \rangle - \langle A_y \sigma_y \rangle + \langle A_z \sigma_z \rangle \leq \sqrt{3}. \quad (8)$$

In the experiment to test the inequalities, Alice prepares two qubits and sends one of them to Bob, who trusts his own measurements but not Alice’s. Bob asks Alice to measure at random σ_x , σ_y , or σ_z on her qubit or simply not to perform any measurement; then Bob measures σ_x , σ_y , or σ_z on his qubit according to Alice’s measurement. Finally, Bob evaluates the average values $\langle \sigma_x \otimes \sigma_x \rangle$, $\langle \sigma_y \otimes \sigma_y \rangle$, $\langle \sigma_x \otimes \sigma_y \rangle$, $\langle \sigma_y \otimes \sigma_x \rangle$, $\langle \sigma_x \otimes \sigma_z \rangle$, and $\langle \mathbb{1} \otimes \sigma_z \rangle$ and is therefore capable of checking whether the steering inequality (7) is violated or not. In particular, for the case of pure states Eq. (1), if Alice is honest in the preparation and measurements of the states, the inequalities are violated for all values of α and φ (except at $\alpha = 0, \pi/2$), thereby confirming Alice’s ability to steer Bob.

4. EXPERIMENTAL RESULTS

The experimental setup is shown in Fig. 1. The degenerated polarization-entangled photon pairs are created by spontaneous parametric down-conversion [29] type-II barium borate (BBO) crystal pumped by a 404 nm laser. The initial two-photon state is singlet state $|\psi\rangle = (|HV\rangle - |VH\rangle)/\sqrt{2}$. By setting half-wave plate (HWP1) at 0° (corresponding to a phase gate), one may switch the phase of the entangled state from “minus” to “plus.” HWP2, HWP3, and beam displacers (BDs) are used to construct an asymmetric loss interferometer to adjust the amplitude and flip the qubit, where HWP3 is fixed at 45°

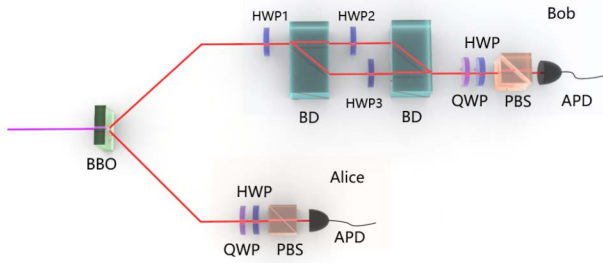


Fig. 1. Experimental setup. Polarization-entangled photons pairs are generated via nonlinear crystal. An asymmetric loss interferometer along with half-wave plates (HWPs) is used to prepare two-qubit pure entangled states. The projective measurements are performed using wave plates and polarization beam splitter (PBS).

and HWP2 at $\arcsin(\sqrt{\frac{1}{\sin^2\alpha} - 1}) \cdot \frac{90}{\pi} \in [0, 45^\circ]$. Therefore, we may prepare the desired two-qubit state as $|\Psi(\alpha)\rangle = \cos\alpha|HH\rangle + \sin\alpha|VV\rangle$ (see Appendix C). Now we define $|H\rangle = |0\rangle$ and $|V\rangle = |1\rangle$, and the entangled state becomes $|\Psi(\alpha)\rangle = \cos\alpha|00\rangle + \sin\alpha|11\rangle$. Compared with Eq. (1), in our experiment, the phase φ of the entangled state is set to zero. As illustrated in Fig. 1, after preparation of the entangled state, we send the first qubit to Alice, and the second to Bob. Then Alice and Bob measure their own photons through the polarization analyzer, which consists of a quarter-wave plate (QWP), HWP, and polarization beam splitter (PBS), and test EPR steering.

First, we test the EPR paradox via steering paradox “ $2 = 1$ ” by choosing α from $\frac{\pi}{36}$ to $\frac{\pi}{4}$ with an interval of $\frac{\pi}{36}$ to obtain nine different two-qubit entangled states. In the two-setting steering scenario, Alice performs measurements on her photon along the \hat{x} direction and \hat{z} direction of the Bloch sphere. The eigenvectors of σ_x are $|\pm\rangle = (|0\rangle \pm |1\rangle)/\sqrt{2}$, which are the states on which Alice’s photon may collapse with a certain probability. The corresponding normalized conditional states for Bob are given by $|\chi_\pm\rangle = \cos\alpha|0\rangle \pm \sin\alpha|1\rangle$. Similarly, Bob’s normalized conditional states are $|0\rangle$ and $|1\rangle$ when Alice performs corresponding measurements. As shown in Fig. 2(a), the experimental values $S = P_{\text{total}}^Q$ for the nine different entangled pure states largely exceed the classical prediction. The average value is $S \approx 1.9899$, which far exceeds the classical bound predicted by LHS models. Thus, the steering paradox has been successfully demonstrated.

Second, we experimentally address the violations of the GLSI using the above pure states $|\Psi(\alpha)\rangle$. We experimentally evaluate the value of S'_3 by using the three-setting steering inequality (7). For simplicity, in our experiment, the phase ϕ is set to zero, and therefore, following the inequality (7), we need to measure only the following four expectation values: $\langle\sigma_x \otimes \sigma_x\rangle$, $\langle\sigma_y \otimes \sigma_y\rangle$, $\langle\sigma_z \otimes \sigma_z\rangle$, and $\langle\sigma_I \otimes \sigma_z\rangle$. To experimentally observe the violation of the GLSI for any $\alpha \in (0, \pi/4]$, we have to maximize the difference between S'_3 and classical bound C'_{LHS} at any fixed value α . This is done by numerically solving the optimal solutions of θ . Remarkably, for $\alpha \in (0, (\arcsin(\frac{\sqrt{3}-1})/2) \approx \frac{\pi}{17}]$, one observes a significant violation of the inequality, which does not occur for the usual

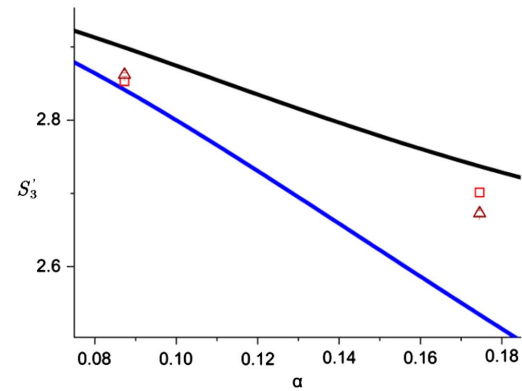
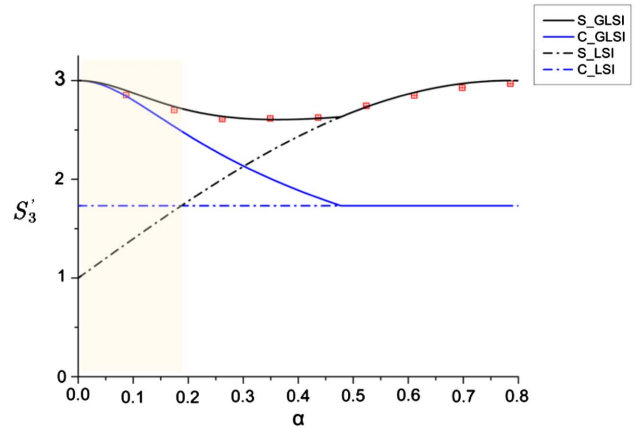
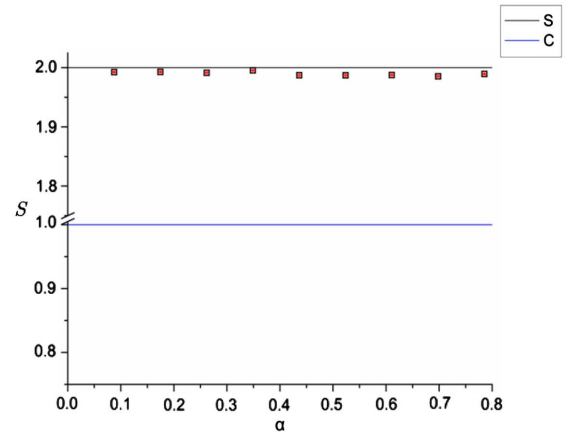


Fig. 2. Experimental results for pure states. (a) Experimental results concerning the steering paradox “ $2 = 1$.” The black and blue solid lines represent the quantum prediction $S \equiv P_{\text{total}}^{\text{QM}} = 2$ and the classical bound $C = 1$ based on the LHV models, respectively. The black cubes and the red lines show the experimental results with error bar. (b) Experimental results for the three-setting GLSI (7). The black and blue solid lines represent the quantum and classic bounds, respectively, which are obtained by maximizing the difference between S'_3 and C'_{LHS} for any fixed α . The black (blue) dot line represents the quantum violation $\langle S'_3 \rangle = 1 + 2 \sin 2\alpha$ (classical value $C = \sqrt{3}$) of the usual three-setting LSI (8). The red cubes are the experimental points for the inequality (7). The light yellow range is $\alpha \in (0, (\arcsin(\frac{\sqrt{3}-1})/2)]$, where the LSI (8) cannot detect the steerability but the GLSI can. (c) Experimental violation for $\alpha = \frac{\pi}{36}, \frac{\pi}{18}$.

three-setting LSI (8). On the other hand, when α is close to $\pi/4$, the violations of the GLSI (7) and the LSI (8) are of the same order. The experimental results are shown in Figs. 2(b) and 2(c), which are almost indistinguishable from theoretical predictions.

Finally, we have experimentally tested inequality (7) with two types of mixed states (see Appendix C). The first one is a generalized Werner state ρ_1 [30], and the second is the asymmetric mixed state ρ_2 [31], which are given as

$$\rho_1 = V|\Psi(\alpha)\rangle\langle\Psi(\alpha)| + \frac{1-V}{4}\mathbb{1} \otimes \mathbb{1}, \tag{9a}$$

$$\rho_2 = V|\Psi(\alpha)\rangle\langle\Psi(\alpha)| + (1-V)|\Phi(\alpha)\rangle\langle\Phi(\alpha)|, \tag{9b}$$

with $|\Phi(\alpha)\rangle = \sin \alpha|01\rangle + \cos \alpha|10\rangle$, $\alpha \in [0, \frac{\pi}{4}]$, and $V \in [0, 1]$. As is apparent in Figs. 3(a) and 3(b), the experimental results confirm that the GLSI has an advantage over the LSI in detecting steerability for more quantum states (see Appendix B for more theoretical details).

5. CONCLUSION

In summary, we have advanced the study of the EPR paradox in two aspects. (i) We have presented a generalized steering paradox “ $k = 1$ ” and performed an experiment to illustrate the original EPR paradox by demonstrating the steering paradox “ $2 = 1$ ” in a two-qubit scenario. (ii) Based on the steering paradox “ $k = 1$,” we have successfully generated a k -setting

GLSI, which may detect steerability of quantum states to a larger extent than previous ones. We have also rewritten this inequality into a mathematically equivalent form, which is more suitable for experimental implementation since it allows us to measure only along the x, y , or z axis in the Bloch sphere, rather than other arbitrary directions, thus greatly simplifying the experimental setups and improving precision. This finding is valuable for the open problem of how to optimize the measurement settings for steering verification in experiments [32]. Our results deepen the understanding of quantum foundations and provide an efficient way to detect the steerability of quantum states.

Recently, quantum steering has been applied to the one-sided device-independent quantum key distribution protocol to secure shared keys by measuring the quantum steering inequality [33]. Our GLSI can also be applied to this scenario to implement the one-sided device-independent quantum key distribution (one-sided DIQKD). In addition, our results may be applied to applications such as quantum random number generation [34,35] and quantum sub-channel discrimination [36,37].

APPENDIX A: GENERALIZED LINEAR STEERING INEQUALITY OBTAINED FROM THE GENERAL STEERING PARADOX “ $k = 1$ ”

Actually, from the steering paradox “ $k = 1$,” one can naturally derive a k setting GLSI, which includes the usual LSI [15] as a special case.

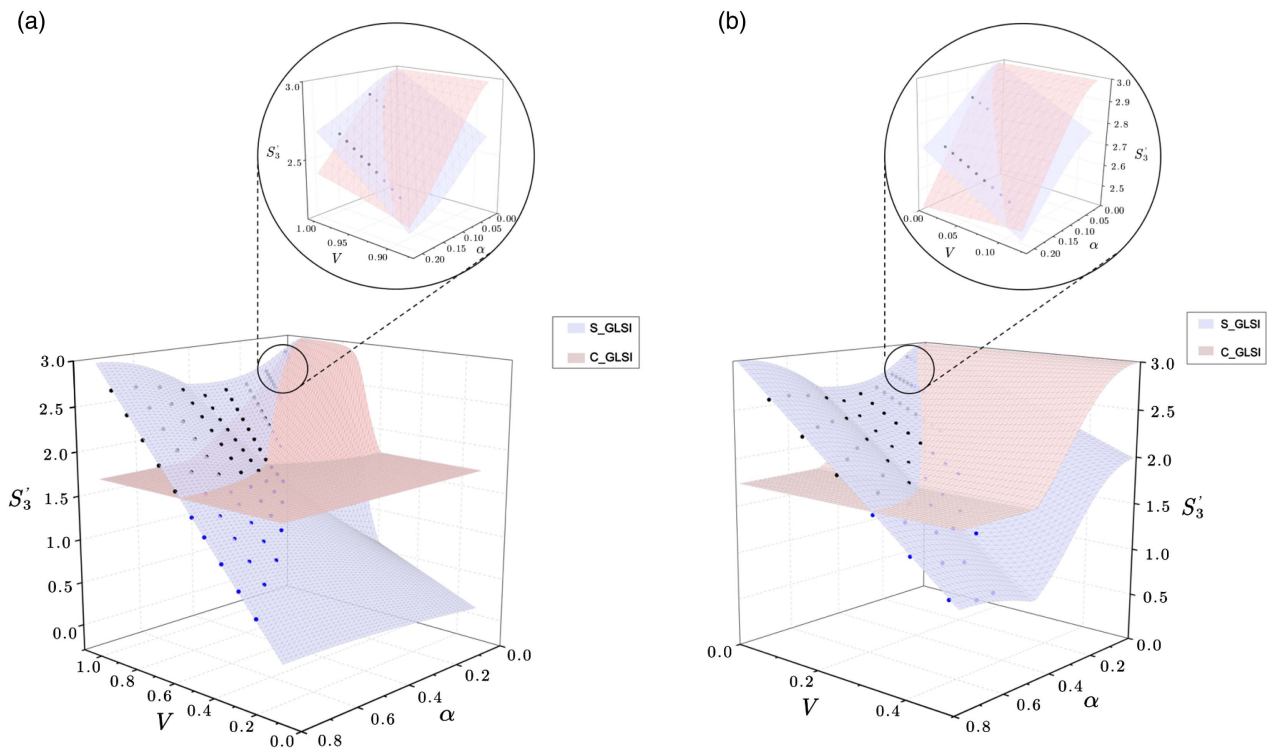


Fig. 3. Experimental results for mixed states. (a), (b) Steering detection for the generalized Werner state ρ_1 and the asymmetric mixed state ρ_2 . The light purple and pink surfaces represent the quantum value and the classical bound of the GLSI (7), respectively. The black (blue) dots denote results for the quantum states that can (cannot) experimentally violate the GLSI (7). The zoom shows the area where steering cannot be detected by usual LSI (8), whereas GLSI may be useful.

The derivation procedure is as follows: in the steering scenario $\{\hat{n}_1, \hat{n}_2, \dots, \hat{n}_k\}$, Alice performs k projective measurements $\hat{P}_a^{\hat{n}_j}$. For the pure state $|\Psi(\theta, \phi)\rangle$ as shown in Eq. (1), it can have an equivalent but more general decomposition along the \hat{n} direction as in Eq. (2). Explicitly, Alice's projective measurements could be rewritten as

$$\hat{P}_0^{\hat{n}_j} = \frac{\mathbb{1} + \hat{n}_j \cdot \vec{\sigma}}{2} = |+\hat{n}_j\rangle\langle+\hat{n}_j|, \quad (\text{A1a})$$

$$\hat{P}_1^{\hat{n}_j} = \frac{\mathbb{1} - \hat{n}_j \cdot \vec{\sigma}}{2} = |-\hat{n}_j\rangle\langle-\hat{n}_j|. \quad (\text{A1b})$$

Based on the two-qubit pure state $|\Psi(\theta, \phi)\rangle$, for the j th projective measurement $\hat{P}_a^{\hat{n}_j}$ of Alice, Bob will have the unnormalized conditional states as

$$\tilde{\rho}_0^{\hat{n}_j} = \text{tr}_A[(\hat{P}_0^{\hat{n}_j} \otimes \mathbb{1})|\Psi\rangle\langle\Psi|] = |\chi_{+\hat{n}_j}\rangle\langle\chi_{+\hat{n}_j}|, \quad (\text{A2a})$$

$$\tilde{\rho}_1^{\hat{n}_j} = \text{tr}_A[(\hat{P}_1^{\hat{n}_j} \otimes \mathbb{1})|\Psi\rangle\langle\Psi|] = |\chi_{-\hat{n}_j}\rangle\langle\chi_{-\hat{n}_j}|, \quad (\text{A2b})$$

from which one has the normalized conditional states as

$$\rho_0^{\hat{n}_j} = \frac{\tilde{\rho}_0^{\hat{n}_j}}{\text{tr}(\tilde{\rho}_0^{\hat{n}_j})} = |\chi_+^j\rangle\langle\chi_+^j|, \quad (\text{A3a})$$

$$\rho_1^{\hat{n}_j} = \frac{\tilde{\rho}_1^{\hat{n}_j}}{\text{tr}(\tilde{\rho}_1^{\hat{n}_j})} = |\chi_-^j\rangle\langle\chi_-^j|, \quad (\text{A3b})$$

with

$$|\chi_+^j\rangle = \frac{|\chi_{+\hat{n}_j}\rangle}{\sqrt{\text{tr}[|\chi_{+\hat{n}_j}\rangle\langle\chi_{+\hat{n}_j}|]}}, \quad (\text{A4})$$

$$|\chi_-^j\rangle = \frac{|\chi_{-\hat{n}_j}\rangle}{\sqrt{\text{tr}[|\chi_{-\hat{n}_j}\rangle\langle\chi_{-\hat{n}_j}|]}}, \quad (\text{A5})$$

being pure states. Obviously, for the pure state $|\Psi\rangle$, the following probability relation always holds:

$$\begin{aligned} & \text{tr}[(\hat{P}_0^{\hat{n}_j} \otimes |\chi_+^j\rangle\langle\chi_+^j|)|\Psi\rangle\langle\Psi|] + \text{tr}[(\hat{P}_1^{\hat{n}_j} \otimes |\chi_-^j\rangle\langle\chi_-^j|)|\Psi\rangle\langle\Psi|] \\ &= \text{tr}[|\chi_{+\hat{n}_j}\rangle\langle\chi_{+\hat{n}_j}|] + \text{tr}[|\chi_{-\hat{n}_j}\rangle\langle\chi_{-\hat{n}_j}|] \equiv 1. \end{aligned} \quad (\text{A6})$$

The quantity on the left-hand-side of Eq. (A6) can be used to construct the steering inequality, whereas for Alice's side, we need to replace the quantum measurement operator $\hat{P}_a^{\hat{n}_j}$ by its corresponding classical probabilities $P(A_{n_j} = a)$. Then we immediately have the k -setting GLSI as

$$\mathcal{S}_k = \sum_{j=1}^k \left[\sum_{a=0}^1 P(A_{n_j} = a) \langle \rho_a^{\hat{n}_j} \rangle \right] \leq C_{\text{LHS}}, \quad (\text{A7})$$

where $P(A_j = a)$ is the classical probability of the j th measurement of Alice with outcome a ,

$$\rho_0^{\hat{n}_j} = |\chi_+^j\rangle\langle\chi_+^j|, \quad \rho_1^{\hat{n}_j} = |\chi_-^j\rangle\langle\chi_-^j| \quad (\text{A8})$$

denote the projective measurements on Bob's side, and C_{LHS} is the classical bound determined by the maximal eigenvalue of the steering parameter \mathcal{S}_k . By definition, it is easy to verify

directly that for the pure state Eq. (1), the quantum prediction of \mathcal{S}_k is equal to k .

Remark 1. In Ref. [15], the usual k -setting LSI is given as

$$\mathcal{S}_k^{\text{LSI}} = \sum_{j=1}^k A_j \langle \hat{m}_j \cdot \vec{\sigma} \rangle \leq C_{\text{LHS}}^{\text{LSI}}, \quad (\text{A9})$$

where $C_{\text{LHS}}^{\text{LSI}}$ denotes the classical bound for the LSI. Note that for the LSI (A9), quantum mechanical Alice will perform k measurements (corresponding to $\hat{A}_j = \hat{n}_j \cdot \vec{\sigma}$), and Bob will also perform k measurements (corresponding to $\hat{B}_j = \hat{m}_j \cdot \vec{\sigma}$). In the following, we show that the LSI is a special case of the GLSI as given in the inequality (A7).

Let us rewrite the projective measurements Eq. (A8) in the Bloch representation as

$$\begin{aligned} \rho_0^{\hat{n}_j} &= |\chi_+^j\rangle\langle\chi_+^j| = \frac{1}{2}(\mathbb{1} + \hat{m}_+^j \cdot \vec{\sigma}), \\ \rho_1^{\hat{n}_j} &= |\chi_-^j\rangle\langle\chi_-^j| = \frac{1}{2}(\mathbb{1} + \hat{m}_-^j \cdot \vec{\sigma}), \end{aligned} \quad (\text{A10})$$

and denote

$$P(A_j = 0) = \frac{1 + A_j}{2}, \quad P(A_j = 1) = \frac{1 - A_j}{2}. \quad (\text{A11})$$

Then by substituting Eqs. (A10) and (A11) into the inequality (A7), we have

$$\begin{aligned} \mathcal{S}_k &= \sum_{j=1}^k \left[\frac{1 + A_j}{2} \langle \frac{1}{2}(\mathbb{1} + \hat{m}_+^j \cdot \vec{\sigma}) \rangle \right. \\ &\quad \left. + \frac{1 - A_j}{2} \langle \frac{1}{2}(\mathbb{1} + \hat{m}_-^j \cdot \vec{\sigma}) \rangle \right] \leq C_{\text{LHS}}. \end{aligned} \quad (\text{A12})$$

Note that for the GLSI (A12), quantum mechanical Alice will perform k measurements (corresponding to $\hat{A}_j = \hat{n}_j \cdot \vec{\sigma}$), and Bob will perform $2k$ measurements (corresponding to $\hat{B}_j^+ = \hat{m}_+^j \cdot \vec{\sigma}$ and $\hat{B}_j^- = \hat{m}_-^j \cdot \vec{\sigma}$, if $\hat{m}_+^j \neq \pm \hat{m}_-^j$). In the following, we show that the LSI is a special case of the GLSI as given in the inequality (A7).

Let

$$\hat{n}_j = (\sin \tau \cos \gamma, \sin \tau \sin \gamma, \cos \tau), \quad (\text{A13})$$

and then

$$|+\hat{n}_j\rangle = \begin{pmatrix} \cos \frac{\tau}{2} \\ \sin \frac{\tau}{2} e^{i\gamma} \end{pmatrix}, \quad |-\hat{n}_j\rangle = \begin{pmatrix} \sin \frac{\tau}{2} \\ -\cos \frac{\tau}{2} e^{i\gamma} \end{pmatrix}, \quad (\text{A14})$$

which are eigenstates of $\hat{n}_j \cdot \vec{\sigma}$. From Eq. (2), one can explicitly have

$$\begin{aligned} |\chi_{+\hat{n}_j}\rangle &= \langle +\hat{n}_j | \Psi(\theta, \phi) \rangle \\ &= \cos \frac{\tau}{2} \cos \theta |0\rangle + e^{i(\phi-\gamma)} \sin \frac{\tau}{2} \sin \theta |1\rangle, \end{aligned} \quad (\text{A15})$$

$$\begin{aligned} |\chi_{-\hat{n}_j}\rangle &= \langle -\hat{n}_j | \Psi(\theta, \phi) \rangle = \sin \frac{\tau}{2} \cos \theta |0\rangle \\ &\quad - e^{i(\phi-\gamma)} \cos \frac{\tau}{2} \sin \theta |1\rangle, \end{aligned} \quad (\text{A16})$$

which yields

$$\langle \chi_{-\hat{n}_j} | \chi_{+\hat{n}_j} \rangle = \cos \frac{\tau}{2} \sin \frac{\tau}{2} (\cos^2 \theta - \sin^2 \theta). \quad (\text{A17})$$

Namely, if $\theta = \pi/4$, the states $|\chi_{+\hat{n}_j}\rangle$ and $|\chi_{-\hat{n}_j}\rangle$ are orthogonal, and then from Eq. (A10), one immediately knows that the two Bloch vectors are antiparallel, i.e.,

$$\hat{m}_+^j = -\hat{m}_-^j \equiv \hat{m}^j. \quad (\text{A18})$$

Substituting the relation Eq. (A18) into the inequality (A12), we have

$$S_k = \frac{1}{2} \sum_{j=1}^k (1 + A_j \langle \hat{m}^j \cdot \vec{\sigma} \rangle) \leq C_{\text{LHS}},$$

i.e.,

$$S_k^{\text{LSI}} = \sum_{j=1}^k A_j \langle \hat{m}^j \cdot \vec{\sigma} \rangle \leq 2C_{\text{LHS}} - k, \quad (\text{A19})$$

proving the usual LSI is a special case of the GLSI. In short, for an arbitrary two-qubit pure entangled state $|\Psi(\theta, \phi)\rangle$, one can have a steering paradox “ $k = 1$ ” [25], based on which one can derive a GLSI as shown in the inequality (A7). If one further fixes the parameter θ as $\theta = \pi/4$ [in this case, $|\Psi(\theta = \pi/4, \phi)\rangle$ is the maximally entangled state], then the GLSI reduces to the usual LSI.

Remark 2. We may rewrite the GLSI (A12) in a mathematically equivalent form that is friendlier for experimental implementations. Let us denote

$$\hat{m}_+^j = (m_{+x}^j, m_{+y}^j, m_{+z}^j), \quad \hat{m}_-^j = (m_{-x}^j, m_{-y}^j, m_{-z}^j), \quad (\text{A20})$$

and then from the inequality (A12), one has

$$\begin{aligned} S_k &= \sum_{j=1}^k \left[\frac{1+A_j}{2} \left\langle \frac{1}{2} (\mathbb{1} + \hat{m}_+^j \cdot \vec{\sigma}) \right\rangle + \frac{1-A_j}{2} \left\langle \frac{1}{2} (\mathbb{1} + \hat{m}_-^j \cdot \vec{\sigma}) \right\rangle \right] \\ &= \sum_{j=1}^k \left[\frac{1}{2} + \frac{1+A_j}{4} (\hat{m}_{+x}^j \langle \vec{\sigma}_x \rangle + \hat{m}_{+y}^j \langle \vec{\sigma}_y \rangle + \hat{m}_{+z}^j \langle \vec{\sigma}_z \rangle) \right. \\ &\quad \left. + \frac{1-A_j}{4} (\hat{m}_{-x}^j \langle \vec{\sigma}_x \rangle + \hat{m}_{-y}^j \langle \vec{\sigma}_y \rangle + \hat{m}_{-z}^j \langle \vec{\sigma}_z \rangle) \right] \leq C_{\text{LHS}}. \end{aligned} \quad (\text{A21})$$

The remarkable point for the inequality (A21) is that Bob always measures his particle in three directions of x, y , and z , which not only greatly reduces the number of measurements, but also there is no need to tune the measurement direction to other directions.

APPENDIX B: EPR STEERING BY USING THE THREE-SETTING GLSI

In this experimental work, we demonstrate EPR steering for the two-qubit generalized Werner state by using the GLSI. We focus on the three-setting GLSI. In the steering scenario $\{\hat{x}, \hat{y}, \hat{z}\}$, Alice performs projective measurements on her qubit along \hat{x} , \hat{y} , and \hat{z} directions; from the inequality (A7), one immediately has

$$\begin{aligned} S_3 &= P(A_x = 0) \langle |\chi_+\rangle \langle \chi_+| \rangle + P(A_x = 1) \langle |\chi_-\rangle \langle \chi_-| \rangle \\ &\quad + P(A_y = 0) \langle |\chi'_+\rangle \langle \chi'_+| \rangle + P(A_y = 1) \langle |\chi'_-\rangle \langle \chi'_-| \rangle \\ &\quad + P(A_z = 0) \langle |0\rangle \langle 0| \rangle + P(A_z = 1) \langle |1\rangle \langle 1| \rangle \leq C_{\text{LHS}}, \end{aligned} \quad (\text{B1})$$

with

$$\begin{aligned} |\chi_{\pm}\rangle &= \cos \theta |0\rangle \pm e^{i\phi} \sin \theta |1\rangle, \\ |\chi'_{\pm}\rangle &= \cos \theta |0\rangle \mp ie^{i\phi} \sin \theta |1\rangle. \end{aligned} \quad (\text{B2})$$

One can have

$$\begin{aligned} |\chi_+\rangle \langle \chi_+| &= \frac{1}{2} (\mathbb{1} + \hat{m}_+ \cdot \vec{\sigma}), & |\chi_-\rangle \langle \chi_-| &= \frac{1}{2} (\mathbb{1} + \hat{m}_- \cdot \vec{\sigma}), \\ |\chi'_+\rangle \langle \chi'_+| &= \frac{1}{2} (\mathbb{1} + \hat{m}'_+ \cdot \vec{\sigma}), & |\chi'_-\rangle \langle \chi'_-| &= \frac{1}{2} (\mathbb{1} + \hat{m}'_- \cdot \vec{\sigma}), \\ |0\rangle \langle 0| &= \frac{1}{2} (\mathbb{1} + \sigma_z), & |1\rangle \langle 1| &= \frac{1}{2} (\mathbb{1} - \sigma_z), \end{aligned} \quad (\text{B3})$$

with

$$\begin{aligned} \hat{m}_+ &= (\sin 2\theta \cos \phi, \sin 2\theta \sin \phi, \cos 2\theta), \\ \hat{m}_- &= (-\sin 2\theta \cos \phi, -\sin 2\theta \sin \phi, \cos 2\theta), \\ \hat{m}'_+ &= (\sin 2\theta \sin \phi, -\sin 2\theta \cos \phi, \cos 2\theta), \\ \hat{m}'_- &= (-\sin 2\theta \sin \phi, \sin 2\theta \cos \phi, \cos 2\theta). \end{aligned} \quad (\text{B4})$$

We now come to compute the classical bound C_{LHS} . Because $P(A_i = 0) + P(A_i = 1) = 1$ ($i = x, y, z$), i.e., $P(A_i = 0)$ is exclusive with $P(A_i = 1)$, if $P(A_i = 0) = 1$; then one must have $P(A_i = 1) = 0$. For the inequality (B1), there are in total eight combinations.

(i) $P(A_z = 0) = P(A_x = 0) = P(A_y = 0) = 1$; then the left-hand side of the inequality (B1) is

$$\langle |\chi_+\rangle \langle \chi_+| + |\chi'_+\rangle \langle \chi'_+| + |0\rangle \langle 0| \rangle, \quad (\text{B5})$$

and for such a matrix, its two eigenvalues are

$$\frac{3 + \sqrt{4 - 4 \cos 2\theta + \cos 4\theta}}{2}, \quad (\text{B6})$$

$$\frac{3 - \sqrt{4 - 4 \cos 2\theta + \cos 4\theta}}{2}. \quad (\text{B7})$$

Similarly, for $P(A_z = 0) = P(A_x = 0) = P(A_y = 1) = 1$, $P(A_z = 0) = P(A_x = 1) = P(A_y = 0) = 1$, and $P(A_z = 0) = P(A_x = 1) = P(A_y = 1) = 1$.

(ii) $P(A_z = 1) = P(A_x = 0) = P(A_y = 0) = 1$; then the left-hand side of the inequality (B1) is

$$\langle |\chi_+\rangle \langle \chi_+| + |\chi'_+\rangle \langle \chi'_+| + |1\rangle \langle 1| \rangle, \quad (\text{B8})$$

and for such a matrix, its two eigenvalues are

$$\frac{3 + \sqrt{4 + 4 \cos 2\theta + \cos 4\theta}}{2}, \quad (\text{B9})$$

$$\frac{3 - \sqrt{4 + 4 \cos 2\theta + \cos 4\theta}}{2}. \quad (\text{B10})$$

Similarly, for $P(A_z = 1) = P(A_x = 0) = P(A_y = 1) = 1$, $P(A_z = 1) = P(A_x = 1) = P(A_y = 0) = 1$, and $P(A_z = 1) = P(A_x = 1) = P(A_y = 1) = 1$.

Thus, in summary, the classical bound is given by [here $\theta \in (0, \pi/2)$]

$$C_{\text{LHS}} = \text{Max}\left\{\frac{3 + C_+}{2}, \frac{3 + C_-}{2}\right\}, \quad (\text{B11})$$

with

$$C_{\pm} = \sqrt{4 \pm 4 \cos 2\theta + \cos 4\theta}. \quad (\text{B12})$$

Obviously the classical bound $C_{\text{LHS}} \leq 3$; however, for any two-qubit pure entangled state $|\Psi(\theta, \phi)\rangle$, one has $S_3^{\text{QM}} = 3$; thus any two-qubit pure entangled state violates the steering inequality (B1).

Let

$$P(A_i = 0) = \frac{1 + A_i}{2}, \quad P(A_i = 1) = \frac{1 - A_i}{2}, \quad (\text{B13})$$

where $i = x, y, z$. Substituting Eqs. (B3), (B4), and (B13) into the inequality (B1) and after simplifying, one obtains the equivalent three-setting steering inequality as

$$\begin{aligned} S'_3 &= \sin 2\theta \cos \phi \langle A_x \sigma_x \rangle - \sin 2\theta \cos \phi \langle A_y \sigma_y \rangle \\ &+ \sin 2\theta \sin \phi \langle A_x \sigma_y \rangle + \sin 2\theta \sin \phi \langle A_y \sigma_x \rangle \\ &+ \langle A_z \sigma_z \rangle + 2 \cos 2\theta \langle \sigma_z \rangle \leq C'_{\text{LHS}}, \end{aligned} \quad (\text{B14})$$

with $C'_{\text{LHS}} = \text{Max}\{C_+, C_-\}$. Obviously, by taking $\theta = \pi/4$ and $\phi = 0$, the inequality (B14) reduces to the usual three-setting LSI (an equivalent form) in Ref. [15].

Example 1. Let us consider the two-qubit pure state $|\Psi(\alpha)\rangle = \cos \alpha|00\rangle + \sin \alpha|11\rangle$; its maximal violation value for the usual three-setting steering inequality (8) is $1 + 2 \sin 2\alpha$. Hence, only when $\alpha > \frac{\arcsin(\frac{\sqrt{3}-1}{2})}{2} \approx 0.1873$ can the usual LSI be violated. However, the pure state violates the GLSI (B1) for the whole region $\alpha \in (0, \pi/2)$; thus the GLSI is stronger than the usual LSI in detecting the EPR steerability of pure entangled states.

Example 2. Let us consider the two-qubit generalized Werner state

$$\rho_1 = \rho_{\text{AB}}(\alpha, V) = V|\Psi(\alpha)\rangle\langle\Psi(\alpha)| + \frac{1 - V}{4} \mathbb{1} \otimes \mathbb{1}, \quad (\text{B15})$$

with $\alpha \in [0, \frac{\pi}{4}]$ and $V \in [0, 1]$.

For the state Eq. (B15), we come to compare the performance between the usual three-setting LSI (blue line) and the three-setting GLSI (red line) in Fig. 4. For the usual LSI, the threshold value of the visibility is given by $V_{\text{Min}} = \frac{\sqrt{3}}{1 + 2 \sin 2\alpha} \approx 0.1873$, below which the usual LSI cannot be violated. Namely, it can be concluded that there are no states violating the usual three-setting LSI with the range of $\alpha \in [0, \frac{\arcsin(\frac{\sqrt{3}-1}{2})}{2}]$. However, the three-setting GLSI can detect more steerable states in the region of α and V , which can be calculated numerically. In Figs. 4 and 5, for example, when $\alpha = \frac{\arcsin(\frac{\sqrt{3}-1}{2})}{2} (\approx \frac{\pi}{17})$, there are no states violating the usual three-setting LSI; however, the GLSI still can detect quantum states in the region $V \in [V_{\text{Min}} \approx 0.914, 1]$. In the range of $\alpha \in [\frac{\arcsin(\frac{\sqrt{3}-1}{2})}{2}, \alpha_B]$, $\alpha_B \approx 0.3508 \approx \frac{\pi}{9}$, there exist states violating the usual LSI, but the corresponding lower bound V_{Min} is larger than that of the three-setting GLSI. In the range of

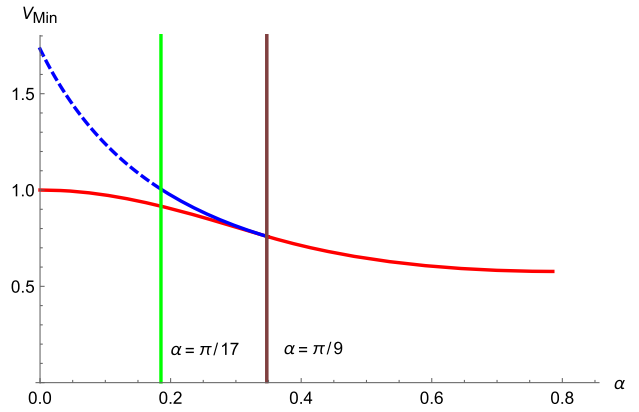


Fig. 4. Detecting EPR steerability of the generalized Werner state by using the usual three-setting LSI (blue line) and three-setting GLSI (red line). For a fixed parameter α , the threshold value of the visibility is given by V_{Min} , below which the steering inequalities cannot be violated. It can be observed that the GLSI is stronger than the usual LSI in detecting EPR steerability.

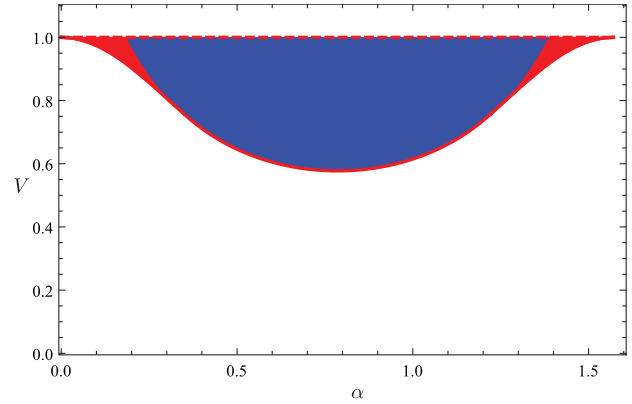


Fig. 5. Generalized Werner states violate the usual three-setting LSI in the blue region and three-setting generalized LSI in the red region. It can be observed that the GLSI is stronger than the usual LSI in detecting EPR steerability.

$\alpha \in [\alpha_B, \frac{\pi}{4}]$, both inequalities are almost equivalent in the task of the steering test. Especially, when $\alpha = \frac{\pi}{4}$, both of them achieve $V_{\text{Min}} = \frac{\sqrt{3}}{3}$.

Example 3. Let us consider the following asymmetric two-qubit mixed state [31]:

$$\rho_2 = V|\Psi(\alpha)\rangle\langle\Psi(\alpha)| + (1 - V)|\Phi(\alpha)\rangle\langle\Phi(\alpha)|, \quad (\text{B16})$$

where $|\Psi(\alpha)\rangle = \cos \alpha|HH\rangle + \sin \alpha|VV\rangle$ and $|\Phi(\alpha)\rangle = \sin \alpha|HV\rangle + \cos \alpha|VH\rangle$. Obviously, ρ_2 is entangled for the region of $\alpha \in (0, \pi/2)$ and $V \in [0, 1/2) \cup (1/2, 1]$.

For the state Eq. (B16), we come to compare the performance between the usual three-setting LSI (blue line) and the three-setting GLSI (red line) in Fig. 6. Because state ρ_2 is unchanged under the operations $V \rightleftharpoons (1 - V)$, and with flipping Alice's states (i.e., $|H\rangle \rightleftharpoons |V\rangle$), the performance in the region $V \in (1/2, 1]$ will be the same as that in the region $V \in [0, 1/2)$. Without loss of generality, we choose the region

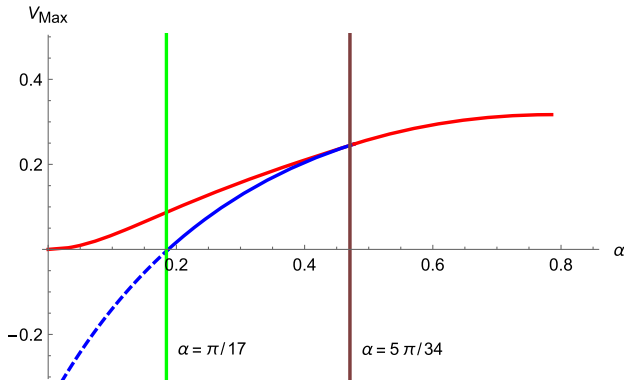


Fig. 6. Detecting EPR steerability of the mixed state Eq. (B16) by using the usual three-setting LSI (blue line) and three-setting GLSI (red line). For a fixed parameter α , the threshold value of the visibility is given by V_{Max} above which the steering inequalities cannot be violated. It can be observed that the GLSI is stronger than the usual LSI in detecting EPR steerability.

of $\alpha \in (0, \pi/2)$ and $V \in [0, 1/2)$; for the usual three-setting LSI, the upper bound $V_{\text{Max}} = \frac{1-\sqrt{3}+2\sin 2\alpha}{2(1+\sin 2\alpha)}$. It is obvious to conclude that there are no states violating the usual three-setting LSI with the range of $\alpha \in [0, \frac{\arcsin(\sqrt{3}-1)}{2} \approx 0.1873]$. However, the three-setting GLSI can detect some more steerable states for a wider region of α and V , which can be calculated numerically. In Figs. 6 and 7, for example, when $\alpha = \frac{\arcsin(\sqrt{3}-1)}{2} (\approx \frac{\pi}{17})$, there are no states violating the usual LSI; however, the GLSI still can detect quantum states in the region $V \in [0, V_{\text{Max}} \approx 0.0889]$. In the range of $\alpha \in [\frac{\arcsin(\sqrt{3}-1)}{2}, \alpha_B]$, $\alpha_B \approx 0.4597 \approx \frac{5\pi}{34}$, there exist some states violating the usual three-setting LSI, but the upper bound V_{Max} is lower than that of the three-setting GLSI. In the range of $\alpha \in [\alpha_B, \frac{\pi}{4}]$, both inequalities are almost equivalent in the task of the steering test. When $\alpha = \frac{\pi}{4}$, both of them achieve $V_{\text{Max}} = \frac{3-\sqrt{3}}{4}$.

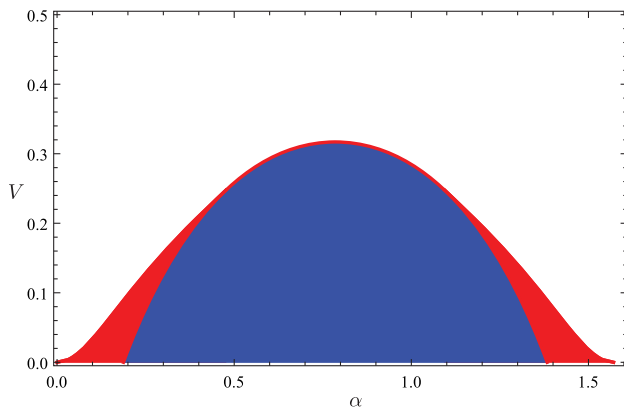


Fig. 7. Mixed states Eq. (B16) violate the usual three-setting LSI in the blue region and three-setting GLSI in the red region. It can be observed that the GLSI is stronger than the usual LSI in detecting EPR steerability.

APPENDIX C: EXPERIMENTAL DETAILS

A 404 nm laser is sent into a nonlinear BBO crystal to generate the maximally entangled state of the form $|\phi\rangle = \frac{1}{\sqrt{2}}(|H\rangle_A|V\rangle_B - |V\rangle_A|H\rangle_B)$ with average fidelity over 99%. By setting HWP1 at 0° , the photon of Bob passes through BD1, which splits the photon into two paths, upper (u) and lower (l), according to its polarization, either vertical (V) or horizontal (H). If HWP2 is rotated by an angle $\frac{\beta}{2}$ and HWP3 is fixed at 45° , the two-photon entangled state becomes

$$|\Psi\rangle = \frac{\sin \beta}{\sqrt{2}}|H\rangle_A|H\rangle_{Bu} - \frac{\cos \beta}{\sqrt{2}}|H\rangle_A|V\rangle_{Bu} + \frac{1}{\sqrt{2}}|V\rangle_A|V\rangle_{Bl}, \quad (\text{C1})$$

where u and l denote upper and lower paths of Bob's photon, respectively. Afterwards, Bob's photon passes through BD2, and the V -polarized element of the entangled state is lost in the upper path. One can verify that the matrix of the process of the asymmetric loss interferometer is

$$\begin{pmatrix} \sin \beta & 0 \\ 0 & 1 \end{pmatrix}, \quad (\text{C2})$$

Therefore, the final state (unnormalized state) is given by

$$|\Psi\rangle = \frac{\sin \beta}{\sqrt{2}}|H\rangle_A|H\rangle_B + \frac{1}{\sqrt{2}}|V\rangle_A|V\rangle_B. \quad (\text{C3})$$

After normalization, the two-qubit entangled state becomes

$$|\Psi\rangle = \frac{\sin \beta}{\sqrt{(\sin \beta)^2 + 1}}|H\rangle_A|H\rangle_B + \frac{1}{\sqrt{(\sin \beta)^2 + 1}}|V\rangle_A|V\rangle_B. \quad (\text{C4})$$

Compared with the form in the main text, by rotating HWP2 by $\beta = \arcsin \left[\sqrt{\frac{1}{(\sin \alpha)^2} - 1} \right] \cdot \frac{90}{\pi} \in [0, 45^\circ]$, we can generate

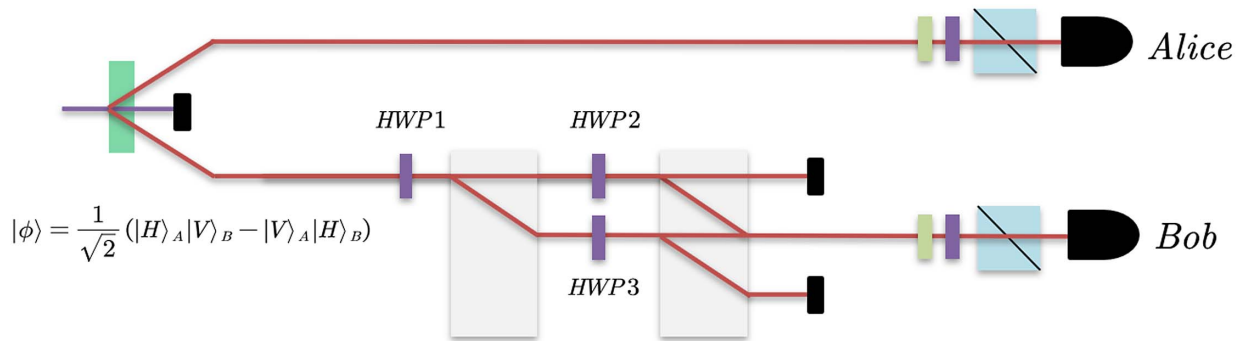
$$|\Psi\rangle = \cos \alpha|H\rangle_A|H\rangle_B + \sin \alpha|V\rangle_A|V\rangle_B. \quad (\text{C5})$$

In our experiments, the verification of the mixed state is achieved by probabilistically mixing the corresponding pure states. Specifically, we measured the corresponding observables in different pure states and post-processed the data (changing the probability of these pure states and mixing them together) to obtain experimental data of different mixed states. Now we show how to construct two types of mixed states, the generalized Werner state, and an asymmetric mixed state [31]:

$$\rho_1 = V|\Psi\rangle\langle\Psi| + (1-V)\frac{\mathbb{1} \otimes \mathbb{1}}{4}, \quad (\text{C6})$$

$$\rho_2 = V|\Psi\rangle\langle\Psi| + (1-V)|\Phi\rangle\langle\Phi|, \quad (\text{C7})$$

where $|\Phi\rangle = \sin \alpha|H\rangle_A|V\rangle_B + \cos \alpha|V\rangle_A|H\rangle_B$, and $V \in [0, 1]$ is the visibility (probability for $|\Psi\rangle\langle\Psi|$). The preparation of the maximally mixed state $\mathbb{1} \otimes \mathbb{1}$ is simulated by mixing the four states $|HH\rangle$, $|HV\rangle$, $|VH\rangle$, and $|VV\rangle$ with equal probability. The generalized Werner state is simulated by mixing $\mathbb{1} \otimes \mathbb{1}$ and $|\Psi\rangle\langle\Psi|$ with probabilities V and $1-V$, respectively. The asymmetric mixed state is simulated by mixing $|\Psi\rangle$



$ H\rangle = 0\rangle; V\rangle = 1\rangle$	HWP1	HWP2	HWP3
$\cos\alpha 0\rangle_A 0\rangle_B + \sin\alpha 1\rangle_A 1\rangle_B$	0°	$\arcsin\left(\sqrt{\frac{1}{\sin^2\alpha}-1}\right) \cdot \frac{90}{\pi} \in [0, 45^\circ]$	45°
$ 0\rangle_A 0\rangle_B$	0°	45°	0°
$ 0\rangle_A 1\rangle_B$	45°	0°	45°
$ 1\rangle_A 0\rangle_B$	45°	45°	0°
$ 1\rangle_A 1\rangle_B$	0°	0°	45°
$\sin\alpha 0\rangle_A 1\rangle_B + \cos\alpha 1\rangle_A 0\rangle_B$	45°	$\arcsin\left(\sqrt{\frac{1}{\sin^2\alpha}-1}\right) \cdot \frac{90}{\pi} \in [45^\circ, 90^\circ]$	

Fig. 8. Experimental setup and the specific angles for state preparation.

and $|\Phi\rangle$ with probabilities V and $1 - V$, respectively. The specific rotation angles of HWP in the BD interferometer for preparing these quantum states are shown in the table in Fig. 8.

Funding. National Key Research and Development Program of China (2017YFA0305200, 2016YFA0301300); National Natural Science Foundation of China (11875167, 12075001, 12075245, 61974168); Key R&D Program of Guangdong Province (2018B030325001, 2018B030329001); Xiaoxiang Scholars Programme of Hunan Normal University.

Disclosures. The authors declare that there are no competing interests.

†These authors contributed equally to this work.

REFERENCES AND NOTES

1. A. Einstein, B. Podolsky, and N. Rosen, "Can quantum-mechanical description of physical reality be considered complete?" *Phys. Rev.* **47**, 777–780 (1935).
2. E. Schrödinger, "Discussion of probability relations between separated systems," *Naturwissenschaften* **23**, 807–812 (1935).
3. H. M. Wiseman, S. J. Jones, and A. C. Doherty, "Steering, entanglement, nonlocality, and the Einstein-Podolsky-Rosen paradox," *Phys. Rev. Lett.* **98**, 140402 (2007).
4. J. S. Bell, "On the Einstein Podolsky Rosen paradox," *Physics* **1**, 195–200 (1964).

5. N. Brunner, D. Cavalcanti, S. Pironio, V. Scarani, and S. Wehner, "Bell nonlocality," *Rev. Mod. Phys.* **86**, 419–478 (2014).
6. J. Clauser, M. Horne, A. Shimony, and R. Holt, "Proposed experiment to test local hidden-variable theories," *Phys. Rev. Lett.* **23**, 880–884 (1969).
7. N. D. Mermin, "Extreme quantum entanglement in a superposition of macroscopically distinct states," *Phys. Rev. Lett.* **65**, 1838–1840 (1990).
8. D. Collins, N. Gisin, N. Linden, S. Massar, and S. Popescu, "Bell inequalities for arbitrarily high-dimensional systems," *Phys. Rev. Lett.* **88**, 040404 (2002).
9. D. M. Greenberger, M. A. Horne, and A. Zeilinger, *Bell's Theorem, Quantum Theory, and Conceptions of the Universe*, M. Kafatos, ed. (Kluwer, 1989), p. 69.
10. L. Hardy, "Nonlocality for two particles without inequalities for almost all entangled states," *Phys. Rev. Lett.* **71**, 1665–1668 (1993).
11. A. Aspect, P. Grangier, and G. Roger, "Experimental tests of realistic local theories via Bell's theorem," *Phys. Rev. Lett.* **47**, 460–463 (1981).
12. J. W. Pan, D. Bouwmeester, M. Daniell, H. Weinfurter, and A. Zeilinger, "Experimental test of quantum nonlocality in three-photon Greenberger–Horne–Zeilinger entanglement," *Nature* **403**, 515–519 (2000).
13. Y. H. Luo, H.-Y. Su, H.-L. Huang, X.-L. Wang, T. Yang, L. Li, N.-L. Liu, J.-L. Chen, C.-Y. Lu, and J.-W. Pan, "Experimental test of generalized Hardy's paradox," *Sci. Bull.* **63**, 1611–1615 (2018).
14. M. D. Reid, P. D. Drummond, E. G. Cavalcanti, W. P. Bowen, P. K. Lam, H. A. Bachor, U. L. Andersen, and G. Leuchs, "The Einstein-Podolsky-Rosen paradox: from concepts to applications," *Rev. Mod. Phys.* **81**, 1727–1751 (2009).
15. D. J. Saunders, S. J. Jones, H. M. Wiseman, and G. J. Pryde, "Experimental EPR-steering using Bell-local states," *Nat. Phys.* **6**, 845–849 (2010).

16. K. Sun, J. S. Xu, X. J. Ye, Y. C. Wu, J. L. Chen, C. F. Li, and G. C. Guo, "Experimental demonstration of the Einstein-Podolsky-Rosen steering game based on the all-versus-nothing proof," *Phys. Rev. Lett.* **113**, 140402 (2014).
17. S. Armstrong, M. Wang, R. Y. Teh, Q. H. Gong, Q. Y. He, J. Janousek, H. A. Bachor, M. D. Reid, and P. K. Lam, "Multipartite Einstein-Podolsky-Rosen steering and genuine tripartite entanglement with optical networks," *Nat. Phys.* **11**, 167–172 (2015).
18. A. J. Bennet, D. A. Evans, D. J. Saunders, C. Branciard, E. G. Cavalcanti, H. M. Wiseman, and G. J. Pryde, "Arbitrarily loss-tolerant Einstein-Podolsky-Rosen steering allowing a demonstration over 1 km of optical fiber with no detection loophole," *Phys. Rev. X* **2**, 031003 (2012).
19. J. Schneeloch, P. B. Dixon, G. A. Howland, C. J. Broadbent, and J. C. Howell, "Violation of continuous-variable Einstein-Podolsky-Rosen steering with discrete measurements," *Phys. Rev. Lett.* **110**, 130407 (2013).
20. M. Fadel, T. Zibold, B. Decamps, and P. Treutlein, "Spatial entanglement patterns and Einstein-Podolsky-Rosen steering in Bose-Einstein condensates," *Science* **360**, 409–413 (2018).
21. F. Dolde, I. Jakobi, B. Naydenov, N. Zhao, S. Pezzagna, C. Trautmann, J. Meijer, P. Neumann, F. Jelezko, and J. Wrachtrup, "Room-temperature entanglement between single defect spins in diamond," *Nat. Phys.* **9**, 139–143 (2013).
22. M. Dabrowski, M. Parniak, and W. Wasilewski, "Einstein-Podolsky-Rosen paradox in a hybrid bipartite system," *Optica* **4**, 272–275 (2017).
23. D. Cavalcanti, P. Skrzypczyk, G. H. Aguilar, R. V. Nery, P. H. S. Ribeiro, and S. P. Walborn, "Detection of entanglement in asymmetric quantum networks and multipartite quantum steering," *Nat. Commun.* **6**, 7941 (2015).
24. Q. Zeng, B. Wang, P. Li, and X. Zhang, "Experimental high-dimensional Einstein-Podolsky-Rosen steering," *Phys. Rev. Lett.* **120**, 030401 (2018).
25. J. L. Chen, H. Y. Su, Z. P. Xu, and A. K. Pati, "Sharp contradiction for local-hidden-state model in quantum steering," *Sci. Rep.* **6**, 32075 (2016).
26. N. D. Mermin, "Quantum mysteries refined," *Am. J. Phys.* **62**, 880–887 (1994).
27. S. H. Jiang, Z. P. Xu, H. Y. Su, A. K. Pati, and J. L. Chen, "Generalized Hardy's paradox," *Phys. Rev. Lett.* **120**, 050403 (2018).
28. For example, the maximal violation value for the usual three-setting steering inequality (8) is $1 + 2 \sin 2\alpha$. Hence, only when $\alpha > \frac{\arcsin \frac{\sqrt{3}-1}{2}}{2} \approx 0.1873$ can the usual LSI be violated. However, the pure state violates the GLSI (7) for the whole region $\alpha \in (0, \pi/2)$; thus, the GLSI is stronger than the usual LSI in detecting the EPR steerability of pure entangled states.
29. P. G. Kwiat, K. Mattle, H. Weinfurter, and A. Zeilinger, "New high-intensity source of polarization-entangled photon pairs," *Phys. Rev. Lett.* **75**, 4337–4341 (1995).
30. E. Wigner, "On the quantum correction for thermodynamic equilibrium," *Phys. Rev.* **40**, 749–760 (1932).
31. J. L. Chen, X. J. Ye, C. Wu, H. Y. Su, A. Cabello, L. C. Kwek, and C. H. Oh, "All-versus-nothing proof of Einstein-Podolsky-Rosen steering," *Sci. Rep.* **3**, 02143 (2013).
32. R. Uola, A. C. S. Costa, H. C. Nguyen, and O. Gühne, "Quantum steering," *Rev. Mod. Phys.* **92**, 015001 (2020).
33. C. Branciard, E. G. Cavalcanti, S. P. Walborn, V. Scarani, and H. M. Wiseman, "One-sided device-independent quantum key distribution: security, feasibility, and the connection with steering," *Phys. Rev. A* **85**, 010301 (2012).
34. P. Skrzypczyk and D. Cavalcanti, "Maximal randomness generation from steering inequality violations using qudits," *Phys. Rev. Lett.* **120**, 260401 (2018).
35. Y. Guo, S. Cheng, X. Hu, B. Liu, E. Huang, Y. Huang, C. Li, G. Guo, and E. G. Cavalcanti, "Experimental measurement-device-independent quantum steering and randomness generation beyond qubits," *Phys. Rev. Lett.* **123**, 170402 (2019).
36. M. Piani and J. Watrous, "Necessary and sufficient quantum information characterization of Einstein-Podolsky-Rosen steering," *Phys. Rev. Lett.* **114**, 060404 (2015).
37. K. Sun, X. Ye, Y. Xiao, X. Xu, Y. Wu, J. Xu, J. Chen, C. Li, and G. Guo, "Demonstration of Einstein-Podolsky-Rosen steering with enhanced subchannel discrimination," *npj Quantum Inf.* **4**, 12 (2018).